The Journal of Immunology

Ezrin Tunes the Magnitude of Humoral Immunity

Debasis Pore, Neetha Parameswaran, Ken Matsui, Matthew B. Stone, Ichiko Saotome, Andrea I. McClatchey, Sarah L. Veatch and Neetu Gupta

J Immunol 2013; 191:4048-4058; Prepublished online 16 September 2013;
doi: 10.4049/jimmunol.1301315
http://www.jimmunol.org/content/191/8/4048

The Journal of Immunology is published twice each month by
The American Association of Immunologists, Inc.,
1451 Rockville Pike, Suite 650, Rockville, MD 20852

Print ISSN: 0022-1767 Online ISSN: 1550-6606.

Ezrin Tunes the Magnitude of Humoral Immunity

Debasis Pore,*[,1] Neetha Parameswaran,*[,1] Ken Matsui,*[,2] Matthew B. Stone,[†] Ichiko Saotome,[‡] Andrea I. McClatchey,[‡] Sarah L. Veatch,[†] and Neetu Gupta*

Ezrin is a member of the ezrin–radixin–moesin family of membrane-actin cytoskeleton cross-linkers that participate in a variety of cellular processes. In B cells, phosphorylation of ezrin at different sites regulates multiple processes, such as lipid raft coalescence, BCR diffusion, microclustering, and endosomal JNK activation. In this study, we generated mice with conditional deletion of ezrin in the B cell lineage to investigate the physiological significance of ezrin's function in Ag receptor–mediated B cell activation and humoral immunity. B cell development, as well as the proportion and numbers of major B cell subsets in peripheral lymphoid organs, was unaffected by the loss of ezrin. Using superresolution imaging methods, we show that, in the absence of ezrin, BCRs respond to Ag binding by accumulating into larger and more stable signaling microclusters. Loss of ezrin led to delayed BCR capping and accelerated lipid raft coalescence. Although proximal signaling proteins showed stronger activation in the absence of ezrin, components of the distal BCR signaling pathways displayed distinct effects. Ezrin deficiency resulted in increased B cell proliferation and differentiation into Ab-secreting cells ex vivo and stronger T cell–independent and -dependent responses to Ag in vivo. Overall, our data demonstrate that ezrin regulates amplification of BCR signals and tunes the strength of B cell activation and humoral immunity. ***The Journal of Immunology*****, 2013, 191: 4048–4058.**

The strength of BCR signaling is a critical determinant of bone marrow B cell development and differentiation into mature subsets in the periphery (1, 2). In mature B cells, the binding of cognate Ag to the BCR initiates multiple signaling pathways that culminate in the production of Ag-specific Abs for immunological protection from pathogens (3). In addition to the essential role of B cells in humoral immunity, Ab-independent functions, including Ag presentation and effector cytokine secretion (4–7), have been identified as important modulators of the immune response. Although BCR signaling is tightly controlled through multiple mechanisms, it can go awry in certain circumstances. For example, BCR signaling is hyperactive in B cells from patients with systemic lupus erythematosus (8) and occurs at a chronic level in certain types of human lymphomas and leukemias (9, 10). High-resolution live cell imaging has revealed that a small proportion of BCRs exist as oligomers in "resting" B cells and that Ag binding to the BCRs initiates their microclustering and recruitment of key proteins for signal transduction (11). Interestingly, certain types of B cell lymphoma, which rely on chronic BCR signaling for survival, exhibit constitutive BCR microclustering (9), indicating a correlation between BCR clustering and signaling. Differences in BCR diffusion and microclustering between resting and activated (11), healthy and diseased (9), IgM- and IgG-expressing B cells (12, 13), and those responding to low- and high-affinity ligands (14, 15) have led to the notion that the outcome of BCR signaling is encoded in differential BCR microclustering behavior and interaction with the plasma membrane (16). Therefore, identification of factors that regulate the formation, growth, and trafficking of BCR microclusters is necessary for a better understanding of B cell behavior in health and disease.

Ezrin is a member of the highly homologous ezrin–radixin–moesin (ERM) family of proteins that possess an N-terminal four-point-one, ezrin, radixin, moesin (FERM) domain and C-terminal actin-binding domain. ERM proteins are highly versatile because they regulate cell motility, protein localization, cellular architecture, and signaling. Phosphorylation of a conserved C-terminal threonine residue is critical for their conformational activation and membrane-actin cross-linking function (17). A role for ezrin in regulating BCR and membrane dynamics was suggested in view of our findings that ezrin responds to BCR ligation by undergoing dephosphorylation at T567, and it facilitates lipid raft coalescence (18). Subsequently, it was shown that expression of dominant negative and constitutively active mutants of ezrin in B cells alters BCR diffusion and Ag gathering (19, 20). Ezrin also undergoes dephosphorylation at T567 in response to chemokine exposure, and this is important for resorption of microvilli and generation of lamellipodia. Thus, ezrin also regulates the morphological and cytoskeletal polarization events that are associated with B cell chemotaxis (21). In addition to its ability to regulate cellular processes that involve plasma membrane–actin cytoskeletal remodeling, ezrin undergoes Syk-dependent phosphorylation at Y353, which enables it to act as a spatial adaptor coupling BCR signaling to JNK activation in the endosomes (22). Furthermore, several recent studies reported a correlation between increased expression and T567 phosphorylation of ezrin and the development of aggressive, metastatic human cancers (23), indicating a significant relationship

*Department of Immunology, Lerner Research Institute, Cleveland Clinic, Cleveland, OH 44195; [†]Department of Biophysics, University of Michigan, Ann Arbor, MI 48109; and [‡]Department of Pathology, Massachusetts General Hospital Cancer Center and Harvard Medical School, Charlestown, MA 02129

[1]D.P. and N.P. contributed equally to this work.

[2]Current address: HPV Immunology Laboratory, Science Applications International Corporation-Frederick, Inc./National Cancer Institute-Frederick, Frederick, MD.

Received for publication May 17, 2013. Accepted for publication August 14, 2013.

This work was supported by Grant AI081743 from the National Institute of Allergy and Infectious Diseases, Grant DK068242 from the National Institute of Diabetes and Digestive and Kidney Diseases, an Investigator Award from the Cancer Research Institute (to N.G.), and Grant GM087810 from the National Institute of General Medical Sciences (to S.L.V.).

Address correspondence and reprint requests to Dr. Neetu Gupta, Department of Immunology, Lerner Research Institute, Cleveland Clinic, 9500 Euclid Avenue, NE40, Cleveland, OH 44195. E-mail address: guptan@ccf.org

Abbreviations used in this article: ASC, Ab-secreting cell; CGG, chicken γ globulin; ERM, ezrin–radixin–moesin; Ez-def, ezrin-deficient; FERM, four-point-one, ezrin, radixin, moesin; MARCH1, membrane-associated ring–CH 1; NP, 4-hydroxy-3-nitrophenyl; STORM, stochastic optical reconstruction microscopy; TIRF, total internal reflection fluorescence.

www.jimmunol.org/cgi/doi/10.4049/jimmunol.1301315

between the expression and active conformation of ezrin and in vivo cellular behavior. These studies underscore the importance of understanding how BCR signaling, B cell activation, and humoral immunity proceed in the absence of ezrin.

In this study, we addressed the role of ezrin in the B cell Ab response by generating conditional knockout mice that lack ezrin expression exclusively in the B cell lineage. We report that the size of BCR microclusters and the magnitude of BCR signaling and Ag-specific Ab production are increased in the absence of ezrin. Our data demonstrate the physiological relevance of ezrin-mediated control of BCR microclustering and membrane dynamics in optimizing the B cell response to Ag.

Materials and Methods

Mice

$Ez^{fl/fl}$ mice (24) were backcrossed with C57BL/6 mice for seven generations before breeding with $MB1^{cre/+}$ mice (25) to generate the $Ez^{fl/fl}$ $MB1^{cre/+}$ mice (ezrin-deficient [Ez-def]). $MB1^{cre/+}$ mice were used as controls in all experiments. All animals were used in compliance with the guidelines approved by the Cleveland Clinic Institutional Animal Care and Use Committee.

Flow cytometry, B cell subset analysis, and immunization

Purified B cells were stained with FITC-, PE- or allophycocyanin-conjugated Abs to surface IgM, CD19, CD21, CD40, CD62L, and ICAM2 (BD Pharmingen) for marker analysis. Developmental stages of B cells and mature B cell subsets were identified based on previously described gating strategies (26). Plasma cells in the bone marrow were identified as $B220^{lo}$ $CD138^{+}$ cells. All flow cytometry data were analyzed using FlowJo software (TreeStar). $MB1^{cre/+}$ and Ez-def mice were immunized with either 50 μg 4-hydroxy-3-nitrophenyl (NP)-Ficoll or 50 μg NP–chicken γ globulin (CGG) along with 10 μg LPS. Sera were collected every week, and NP-specific IgG Abs were quantified by ELISA.

B cell stimulation and immunoblotting

Splenic B and T cells were MACS purified by negative selection (Miltenyi Biotec). B cells were stimulated with 10 or 50 μg/ml (for JNK activation) of anti-IgM or primed with 10 μg/ml LPS for 48 h, followed by stimulation with 10 or 50 μg/ml (for JNK activation) of anti-IgM for the indicated times. Lysates were prepared, and immunoblotting was performed as described (18). To assess cell proliferation, purified B cells were labeled with 1 μM CFSE and stimulated with 10 μg/ml anti-IgM for 5 d. Cells were analyzed every 24 h by flow cytometry, and the number of cells at each division was quantified using FlowJo.

ELISPOT assay

Purified B cells were primed with 0.1 μg/ml LPS for 48 h, followed by stimulation with 10 μg/ml anti-IgM for 24 h, and transferred to ELISPOT plates precoated with unlabeled anti-mouse Ig for 16–18 h at 37°C. The plates were washed, incubated with HRP-conjugated anti-IgM and anti-IgG Abs for 2 h at room temperature, and developed with AEC Chromogen (BD Biosciences). The plates were imaged and analyzed using an Immunospot plate reader (Cellular Technology).

Total internal reflection fluorescence imaging

Purified B cells were labeled with 2 μg/ml Cy5-conjugated goat anti-mouse IgM (μ chain-specific) Fab fragment for 20 min at 4°C. For stimulation, cells were added to glass-bottom petri dishes (MatTek) coated with 10 μg/ml goat anti-mouse IgM (H+L specific) $F(ab')_2$ fragment. Cells were allowed to settle for 2–3 min, and images were collected every 5 s for a period of 15 min. Images were acquired in warm imaging buffer (RPMI 1640 without phenol red, 10% FBS, 2 mM glutamine, 10 mM N-2-hydroxyethylpiperazine-N′-2-ethanesulfonic acid) using a Leica-AM total internal reflection fluorescence (TIRF) microscope DMI6000 (Leica Microsystems) with an attached Hamamatsu EM-CCD camera and Leica acquisition software LAS AF Version 2.2.0. An HCX PL APO 100× oil objective (NA = 1.47) was used at an additional 1.6× magnification with appropriate filter cubes. The images were digitally deconvolved using Metamorph and analyzed further for cluster area, intensity, and velocity with ImagePro Plus 7.0. BCR cluster stability was measured at 8 min of stimulation by quantifying the subsequent number of frames for which each BCR cluster persisted. To test the association of BCRs with tyrosine-phosphorylated proteins (pY), B cells were stimulated with 10 μg/ml biotinylated goat anti-mouse IgM (H+L specific) $F(ab')_2$ fragment for 3 min. Cells were fixed, stained with streptavidin Alexa Fluor 647, permeabilized, and stained with anti-phosphotyrosine Ab (4G10). The surface plane of labeled B cells was imaged by epifluorescence microscopy using the microscope described above. The images were digitally deconvolved and analyzed further for cluster area, intensity, and Pearson correlation coefficient using Volocity 6.0. For BCR-capping studies, B cells were labeled with 25 μg/ml biotinylated goat anti-mouse IgM (H+L specific) $F(ab')_2$ fragment for 20 min. During the labeling period, cells were left unstimulated at 4°C or stimulated at 37°C for 5 and 10 min. Cells were fixed and stained with streptavidin Alexa Fluor 568. To image lipid rafts, B cells were stimulated with 25 μg/ml goat anti-mouse IgM (μ chain-specific) $F(ab')_2$ fragment for 5 and 10 min. Cells were fixed and stained with 0.1 μg/ml Alexa Fluor 488–conjugated cholera toxin subunit B (Molecular Probes) for 15 min at 4°C. B cells were stained with DAPI (Invitrogen) and washed, and image slices were acquired through the *z*-axis with an interval of 0.2 μm. The images were digitally deconvolved and "extended focus" view of the images was generated using Volocity 6.0. "Extended focus" view displays a single image by making a brightest point merge of all the Z-slices of an image volume.

Stochastic optical reconstruction microscopy imaging

Purified B cells were added to glass-bottom wells precoated with poly-D-lysine (MatTek), and surface BCR was stained with 10 μg/ml Alexa Fluor 647 and biotin-labeled Fab fragment of anti-mouse IgM. Cells in Fig. 3A were stimulated for 5 min by addition of 1 μg/ml streptavidin (Life Technologies) and fixed with 4% paraformaldehyde and 0.1% glutaraldehyde (Ted Pella) prior to imaging in fixed cell imaging buffer, as described (27). Cells in Fig. 3C were imaged in live cell imaging buffer (30 mM Tris, 10 mg/ml glucose, 100 mM NaCl, 5 mM KCl, 1 mM $MgCl_2$, 1.8 mM $CaCl_2$, 4 mg/ml glutathione, with 40 μg/ml catalase and 500 μg/ml glucose oxidase [pH 8]). BCR was cross-linked by addition of 1 μg/ml soluble streptavidin, which served to stimulate the cells, as evidenced by calcium response in control cells. Imaging was performed on an Olympus IX81-XDC inverted microscope with a cellTIRF module, a 100× UAPO TIRF objective (NA = 1.49), and active Z-drift correction (Olympus America), using an EMCCD camera (iXon-897; Andor). Excitation and photoswitching of Alexa Fluor 647 was accomplished using 640-nm laser excitation (CUBE 640-74FP; Coherent). Laser intensities were adjusted such that single fluorophores could be distinguished in individual images.

Stochastic optical reconstruction microscopy analysis

Single-molecule fluorescent events were localized by fitting local maxima in background-subtracted images to Gaussian functions using standard methods. Superresolution images were reconstructed from single-molecule localizations, and autocorrelation curves were calculated as described (28). In fixed cells, measured autocorrelation functions were fit to a single exponential, $g(r) = 1 + A\exp(-r/\xi)$, where A is the amplitude, ξ is the characteristic size of clusters, and $\int 2\pi(g(r) - 1)dr = 2\pi A\xi^2$ is proportional to the number of proteins in clusters (28). Single-molecule trajectories were determined using standard tracking algorithms, which search for localizations within 400 nm in subsequent frames and remove ambiguous trajectories. Diffusion coefficients for single-molecule trajectories persisting ≥10 frames (0.1 s) were tabulated by fitting a line to early time points (20–40 ms) of the mean squared displacement curve.

Statistical analysis

All analyses were performed using Prism 4 software (GraphPad Software) using an α-level of 0.05.

Results

B cell development is unaffected by the loss of ezrin

To investigate the physiological role of ezrin in B cell development, Ag-induced activation, and humoral immune response, we bred $Ez^{fl/fl}$ (24) and $MB1^{cre/+}$ (25) mice to generate B cell–specific conditional deletion of ezrin. Loss of ezrin expression in B cells from Ez-def mice was confirmed by Western blotting of lysates (Fig. 1A). Expression of the related protein moesin and its phosphorylation at the regulatory threonine residue were unaffected by the loss of ezrin (Fig. 1A), indicating a lack of compensation. The deletion of ezrin was specific to B cells, because purified splenic T cells from Ez-def and $MB1^{cre/+}$ mice showed similar expression

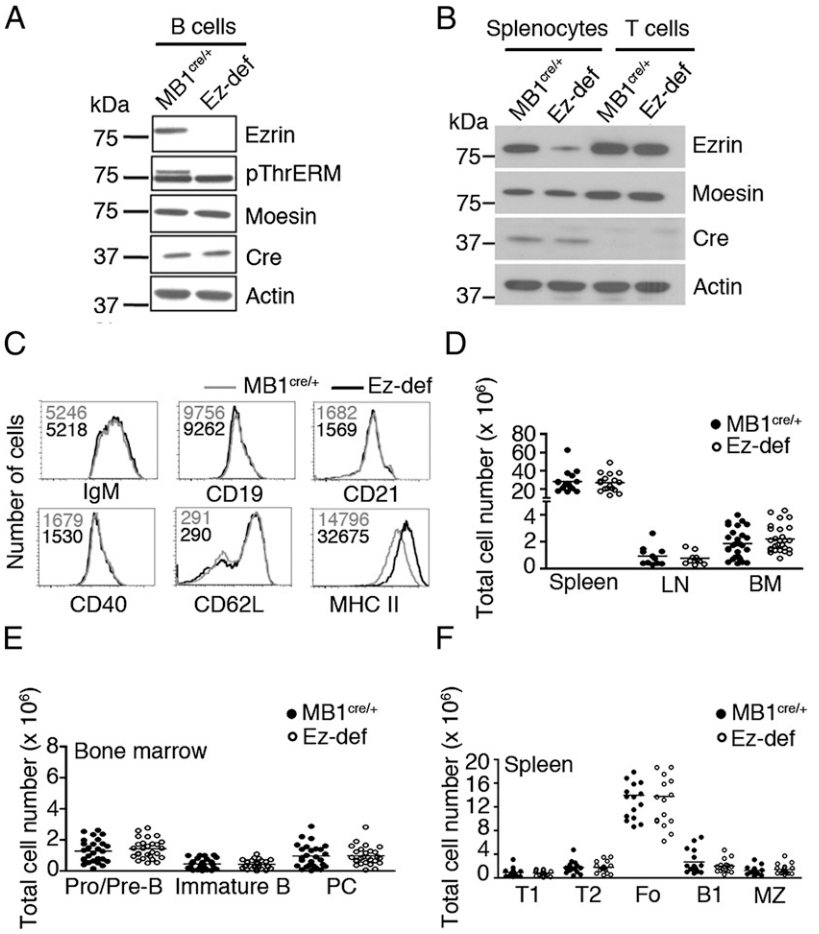

FIGURE 1. Absence of ezrin in B cells does not affect B cell development. Lysates from purified B cells (**A**) or splenocytes and purified T cells (**B**) from MB1$^{cre/+}$ or Ez-def mice were probed for ezrin, pThrERM, moesin, cre recombinase, and actin. (**C**) Expression of indicated surface receptors on purified B cells from MB1$^{cre/+}$ and Ez-def mice. Median fluorescence intensities for the surface proteins are shown for a representative of four independent experiments. (**D**) CD19^{+}IgM^{+} B cells were quantified in the spleen, lymph node (LN), and bone marrow (BM) from MB1$^{cre/+}$ and Ez-def mice. Absolute numbers of pro/pre, immature, and plasma cells (PC) in the bone marrow (**E**) and transitional 1 (T1), transitional 2 (T2), follicular (Fo), B1, and marginal zone (MZ) B cells in the spleen (**F**). Each symbol corresponds to an individual mouse.

of ezrin (Fig. 1B). The absence of ezrin did not alter the steady-state expression level of the BCR (surface IgM) or other important transmembrane receptors, such as CD19, CD21, and CD40. The basal expression of CD62L (L-selectin) was not altered by the absence of ezrin, but expression of MHC class II was 2-fold higher on Ez-def B cells (Fig. 1C). Similar numbers of IgM^{+}CD19^{+} B cells were detected in the spleen, lymph nodes, and bone marrow of MB1$^{cre/+}$ and Ez-def mice (Fig. 1D). The developmental stages of B cells in the bone marrow (Fig. 1E) and the follicular, marginal zone, and B1 mature B cell subsets in the spleen (Fig. 1F) were also unaffected by the loss of ezrin. These data show that ezrin is dispensable for B cell development, homeostasis, and expression of cell surface receptors. However, Ez-def cells appear to be partially preactivated, as indicated by higher basal MHC class II expression.

Absence of ezrin increases the size of Ag-induced BCR microclusters

Because dominant negative and constitutively active mutants of ezrin were reported to alter BCR dynamics (20), we used TIRF microscopy to examine the effect of ezrin deficiency on Ag-induced BCR microclustering in naive B cells. To simulate physiological Ag binding along with innate stimulation through TLRs, we also examined LPS-primed B cells that were stimulated with anti-IgM. As expected, the BCRs clustered in response to immobilized anti-IgM in both naive (Fig. 2A) and LPS-primed (Fig. 2F) B cells from MB1$^{cre/+}$ and Ez-def mice. In naive Ez-def B cells, the clusters occupied a 2-fold larger area (Fig. 2B) and showed increased pixel intensity (Fig. 2C) than in MB1$^{cre/+}$ cells, suggesting that they contained more BCR molecules. The velocity of migration of the BCR clusters was lower in Ez-def B cells (Fig. 2D), causing them to be visualized for a greater number of frames than those in MB1$^{cre/+}$ B cells (Fig. 2E). Like naive B cells, LPS-primed Ez-def B cells also responded to BCR ligation by forming bigger (Fig. 2G), more intense (Fig. 2H), slower (Fig. 2I), and more stable (Fig. 2J) BCR clusters than did LPS-primed MB1$^{cre/+}$ B cells.

Mobility of individual BCRs is reduced in Ez-def B cells

To explore whether the lower velocity of migration of BCR clusters observed in Ez-def cells was indicative of reduced mobility of single BCR molecules, we performed superresolution fluorescence localization microscopy to measure BCR diffusion in live primary cells. This imaging method, frequently referred to as stochastic optical reconstruction microscopy (STORM), exploits the reversible photo-switching capability of cyanine dyes in reducing buffers with low oxygen content (27). Because the reducing nature of the buffer does not allow for stimulation with F(ab′)$_2$ fragment of anti-IgM, soluble streptavidin was used to cross-link biotins conjugated to the labeling Fab anti-IgM Ab (see *Materials and Methods*). To verify that this stimulation method produced BCR clusters with physical properties similar to those stimulated with anti-IgM as in Fig. 2, we imaged BCRs in MB1$^{cre/+}$ and Ez-def cells that were fixed 5 min after stimulation with soluble streptavidin. The representative STORM images shown in Fig. 3A suggested that BCR microclusters were larger in Ez-def cells compared with the control MB1$^{cre/+}$ cells. This visual observation was confirmed by subjecting reconstructed images of multiple cells to quantification using autocorrelation functions, as described previously (28). By this method, we found that the average size of BCR microclusters

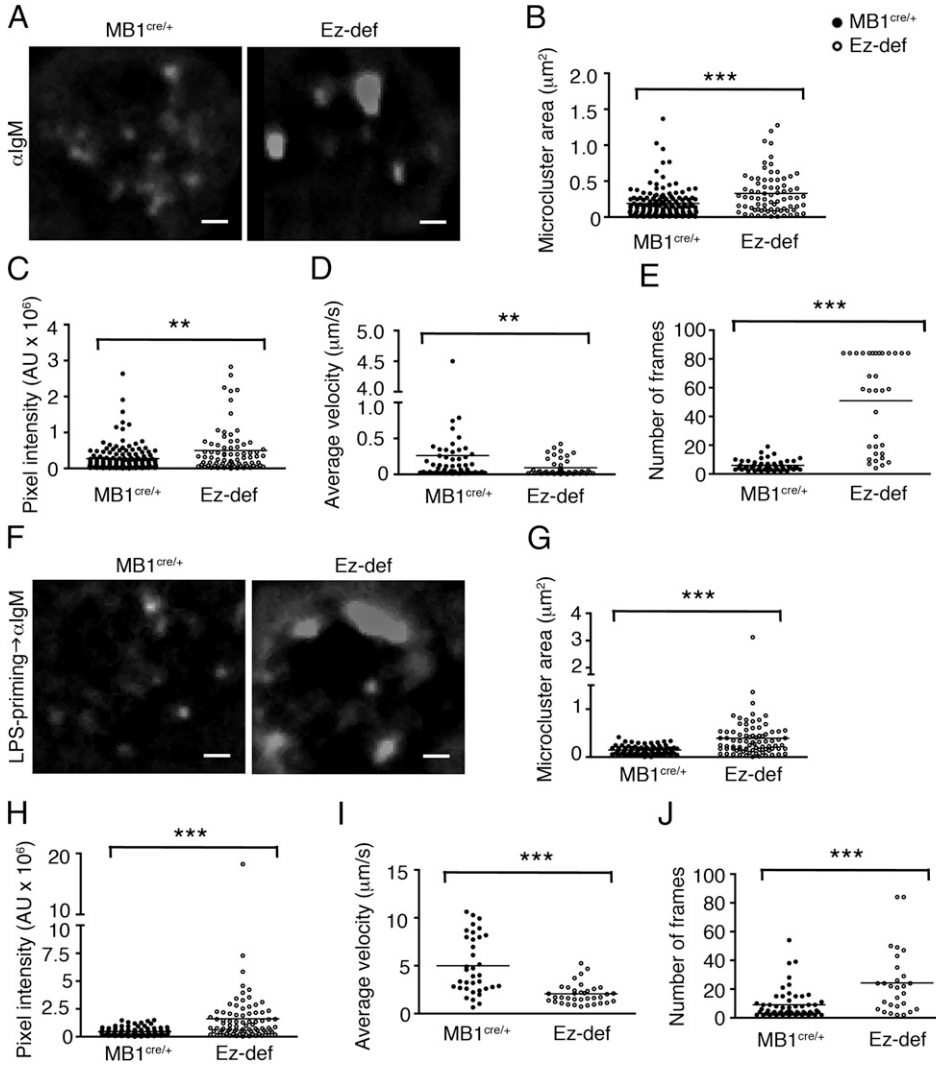

FIGURE 2. Ez-def B cells form bigger, more stable, and slower-moving BCR microclusters upon Ag stimulation. BCRs on naive (**A**) or LPS-primed (**F**) MB1$^{cre/+}$ and Ez-def B cells were imaged live by TIRF microscopy. Still images of BCR clusters formed after 8 min of anti-IgM stimulation are shown. Individual clusters were quantified for area (**B**, **G**), pixel intensity (**C**, **H**), velocity (**D**, **I**), and the number of frames for which the clusters persisted (**E**, **J**). Scale bar, 5 μm. Data are representative of three independent experiments with ~10 cells imaged per experiment and 40–60 individual clusters/experiment analyzed for quantification. $^{**}p = 0.001$–0.01, $^{***}p < 0.001$.

formed upon Ag stimulation was larger in Ez-def B cells ($\xi_{Ez\text{-}def}$ = 90 nm) compared with MB1$^{cre/+}$ cells ($\xi_{MB1cre/+}$ = 65 nm) (Fig. 3B). Ez-def cells also have a greater integral ($I_{Ez\text{-}def}$ = 330,000 versus $I_{MB1cre/+}$ = 290,000), determined from the integrals of fixed-cell BCR correlation functions, indicating that clusters in Ez-def cells contain ~14% more BCRs than do clusters in MB1$^{cre/+}$ cells (Fig. 3B). We note in this study that the images in Fig. 3A and quantification in Fig. 3B are subject to overcounting artifacts, because the Alexa Fluor 647 fluorophore photo-switches reversibly under our imaging conditions (28). In the context of these data, we likely underestimated domain size and overestimated the clustering amplitude for both cell types to roughly the same extent.

Next, we measured the localization and mobility of single BCR proteins in unstimulated and stimulated live B cells. Fig. 3C shows representative images reconstructed from live cell data before Ag addition (*left panels*) and between 5 and 9 min after Ag addition (*right panels*), depicting the time-average positions of localized BCR proteins. Rainbow color-coded single-molecule trajectories are superimposed on these images. The increased number of slower blue trajectories for the Ag-stimulated Ez-def cell in Fig. 3C suggests that the BCRs in Ez-def B cells are less mobile, consistent with observations made with microclusters (Fig. 2D, 2H). Fig. 3D shows the cumulative probability distribution of BCR trajectory diffusion coefficients observed over multiple unstimulated cells and those stimulated between 5 and 9 min. The midpoint of this distribution (cumulative probability = 0.5) indicates the median diffusion coefficient. The median diffusion coefficient of the BCRs for unstimulated MB1$^{cre/+}$ cells (0.16 μm^2/s) and Ez-def cells (0.14 μm^2/s) was similar (Fig. 3D). In contrast, the BCRs exhibited a 2-fold lower diffusion constant in Ag-stimulated Ez-def cells (0.017 μm^2/s) than in MB1$^{cre/+}$ cells (0.034 μm^2/s) (Fig. 3D).

Loss of ezrin in B cells results in delayed BCR capping and accelerated lipid raft coalescence

It is well established that continuous BCR cross-linking leads to progressive patching and polarized capping of the BCRs (3). Because the BCR microclusters appeared to be heavier, slower, and more stable in Ez-def B cells, we tested whether this compromised their ability to aggregate into patches and caps. We stimulated naive MB1$^{cre/+}$ and Ez-def B cells with anti-IgM and stained the surface IgM to visualize its distribution in the absence of stimulation or at 5 and 10 min of stimulation. In this stimulation scheme, B cells showed three types of distribution: mostly uniform, two patches, or fully capped (Fig. 4A). We quantified the fraction of cells displaying each pattern of distribution at different times and observed that, in the unstimulated state, the BCR was uniformly distributed in both MB1$^{cre/+}$ and Ez-def B cells (Fig. 4B). A majority of MB1$^{cre/+}$ and Ez-def B cells showed capped BCRs at 5 min of stimulation, with ~20% showing two patches. At 10 min, 100% of MB1$^{cre/+}$ B cells had fully capped their BCRs,

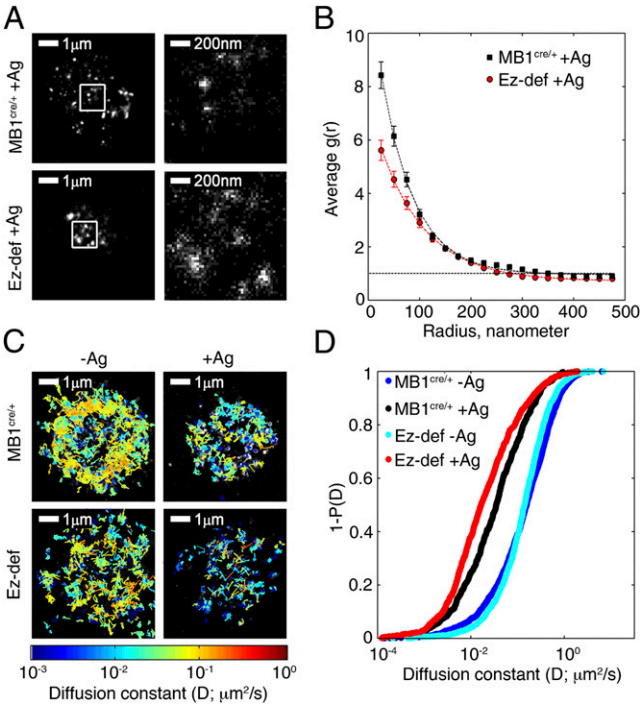

FIGURE 3. BCRs exhibit differential clustering and diffusion in MB1$^{cre/+}$ and Ez-def cells. (**A**) Representative reconstructed superresolution images of BCR in primary cells fixed 5 min after the addition of soluble Ag. Reconstructed images were created by iterating pixel values corresponding to BCR localizations, where the pixel size is 25 nm (approximately the localization resolution). Reconstructed images (*left panels*) were blurred to reduce pixelation. White box in left panel shows the area selected for higher magnification (*right panels*). (**B**) BCR clustering is quantified from multiple images like those shown in (A) using correlation functions tabulated from all MB1$^{cre/+}$ and Ez-def cells. Line shown is a fit to g(r)=A× e-r/ξ + offset, where ξ is a measure of the characteristic size of BCR clusters. Additionally, the integral under this curve ($I = 2\pi A\xi^2$) is related to the average number of correlated probes present within clusters. (**C**) Representative reconstructed superresolution images of BCR in live primary cells collected for 5 min prior to Ag stimulation (-Ag) or between 5 and 9 min following Ag stimulation (+Ag). BCR trajectories are overlaid on images and are rainbow color-coded according to their best-fit diffusion coefficient, with red representing the most mobile and blue representing the least mobile. (**D**) Cumulative distribution of single BCR diffusion coefficients observed in multiple cells under the same conditions described in (C).

but 20% of Ez-def B cells still showed two patches (Fig. 4B). These data indicate that the slower motility and increased stability of BCR clusters and patches may have prevented them from forming polarized caps in the absence of ezrin. We demonstrated previously that Ag-induced dephosphorylation of ezrin at the conserved T567 residue causes it to dissociate from lipid rafts and the cortical actin, and this facilitates lipid raft coalescence (18). Expression of a phosphomimetic mutant of ezrin irreversibly links rafts with F-actin and prevents raft coalescence (18). This led us to predict that loss of ezrin would release lipid rafts from the constraint imposed by membrane-actin cross-linking and may affect their aggregation. We tested this by stimulating MB1$^{cre/+}$ and Ez-def B cells with anti-IgM for different times and visualizing lipid rafts with fluorescent cholera toxin B. At each time of stimulation, B cells exhibited three patterns of lipid raft staining (Fig. 4C). Lipid rafts were punctate but not coalesced, partially coalesced, or fully coalesced (capped) (Fig. 4C). The fraction of MB1$^{cre/+}$ and Ez-def B cells displaying each of these patterns was comparable in the absence of anti-IgM stimulation (Fig. 4D). After 5 min of stimulation, none of the Ez-def B cells had noncoalesced rafts, whereas ~10% of MB1$^{cre/+}$ cells still showed noncoalesced rafts. Seventy percent of Ez-def B cells showed fully coalesced rafts compared with 50% of MB1$^{cre/+}$ B cells at 5 min (Fig. 4D). At 10 min of anti-IgM cross-linking, only 20% of Ez-def B cells had partially coalesced rafts at 10 min, whereas 50% of MB1$^{cre/+}$ cells still showed this pattern of distribution. Eighty percent of Ez-def had fully coalesced rafts at this time as opposed to 50% of MB1$^{cre/+}$ cells. These data indicate that Ag-induced lipid raft coalescence is enhanced in the absence of ezrin. Overall, our data suggest that greater stability of BCR clusters, delayed BCR capping, and increased raft coalescence may promote stronger signaling in Ez-def B cells than in MB1$^{cre/+}$ B cells.

Loss of ezrin in B cells leads to increased recruitment of tyrosine-phosphorylated proteins to BCR microclusters

Because clustering and slowing of BCRs is associated with signal transduction (11), we examined the relative ability of MB1$^{cre/+}$ and Ez-def B cells to undergo BCR-mediated activation. We first tested whether the larger BCR clusters formed upon antigenic stimulation in the absence of ezrin were passive or associated with signaling capacity. Because the BCR interacts with tyrosine-phosphorylated proteins upon cross-linking, we simultaneously imaged the BCR and phosphotyrosine-containing proteins in the epifluorescence mode in fixed and permeabilized MB1$^{cre/+}$ and Ez-def B cells that had been stimulated with anti-IgM for 3 min. Phosphotyrosine staining was barely detectable in unstimulated MB1$^{cre/+}$ and Ez-def B cells, but it was robustly induced upon anti-IgM stimulation (Fig. 5A). The BCR clusters formed in Ez-def B cells were larger than in MB1$^{cre/+}$ B cells, as seen before, and were associated with phosphotyrosine-containing proteins (Fig. 5A). The intensity of phosphotyrosine associated with BCR clusters was higher in Ez-def B cells than in MB1$^{cre/+}$ B cells (Fig. 5B), indicating an increased signaling capacity of the larger clusters in Ez-def B cells. Furthermore, the correlation between BCRs and phosphotyrosine-containing proteins was stronger in Ez-def B cells than in MB1$^{cre/+}$ B cells (Fig. 5C).

Proximal BCR signaling is stronger in the absence of ezrin

Next, we stimulated naive or LPS-primed B cells with anti-IgM to compare the profile of tyrosine-phosphorylated proteins in MB1$^{cre/+}$ and Ez-def B cells. Both naive and LPS-primed Ez-def B cells showed an increase in band intensity of many tyrosine-phosphorylated proteins (indicated by arrows) compared with MB1$^{cre/+}$ cells (Fig. 6), indicating a global increase in proximal BCR signaling. To identify the proteins that underwent higher phosphorylation, we performed targeted immunoblotting analysis of key proximal signaling proteins. We chose to test phosphorylation of Igα, which is the earliest target of Src family kinase activation, Syk tyrosine kinase, which is recruited to the BCR and phosphorylates downstream targets, and PLCγ, whose activity regulates protein kinase C activation and calcium signaling. Naive or LPS-primed B cells from MB1$^{cre/+}$ and Ez-def mice were stimulated with anti-IgM, and lysates were probed with phospho-specific Abs to Igα, Syk, and PLCγ. All three proteins showed higher phosphorylation in lysates of Ez-def B cells compared with MB1$^{cre/+}$ B cells (Fig. 6), indicating that absence of ezrin increases proximal BCR signaling.

Absence of ezrin has distinct effects on different components of distal BCR signaling pathways

To test whether a higher magnitude of tyrosine phosphorylation impacts downstream effector pathways, we investigated the effect of ezrin deficiency on the activation of MAPKs ERK, p38, and

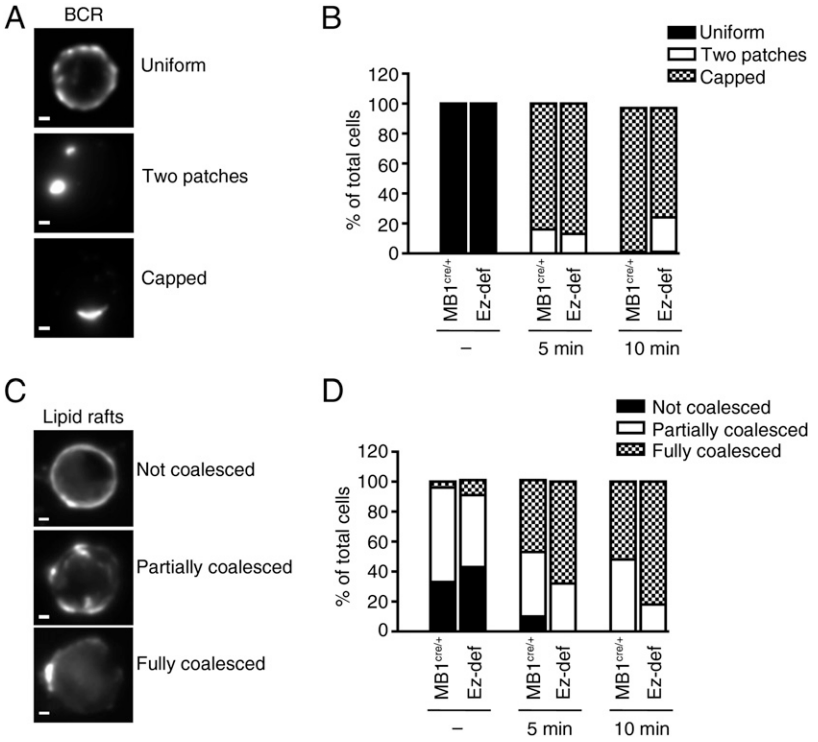

FIGURE 4. Ezrin deficiency results in delayed BCR capping and accelerated lipid raft coalescence. MB1$^{cre/+}$ and Ez-def B cells were stimulated with 25 μg/ml anti-IgM for 5 and 10 min, stained for BCR (**A**) or lipid rafts (**B**), and imaged by epifluorescence microscopy. The most prominent distributions displayed by the BCR (A) and lipid rafts (B) are shown as extended focus images of representative cells. Scale bar, 1 μm. Stacked bar graphs depict the percentage of cells displaying each type of distribution for BCR (**C**) and lipid rafts (**D**) at indicated times. Data are representative of two independent experiments, with 20–25 cells imaged per experiment.

JNK, as well as PI3K. Anti-IgM–induced phosphorylation of ERK was higher in both naive and LPS-primed Ez-def B cells compared with MB1$^{cre/+}$ B cells (Fig. 7). The loss of ezrin had no effect on phosphorylation of p38 or on Akt, which is a reporter of PI3K activity (Fig. 7). We showed previously that Y353-phosphorylated ezrin couples proximal BCR signaling to endosomal JNK activation, suggesting a positive regulatory role for ezrin in this pathway (22). As expected, anti-IgM–induced JNK phosphorylation was lower in naive Ez-def B cells compared with MB1$^{cre/+}$ B cells (Fig. 7A). However, LPS-primed MB1$^{cre/+}$ and Ez-def B cells showed similar activation of JNK (Fig. 7B).

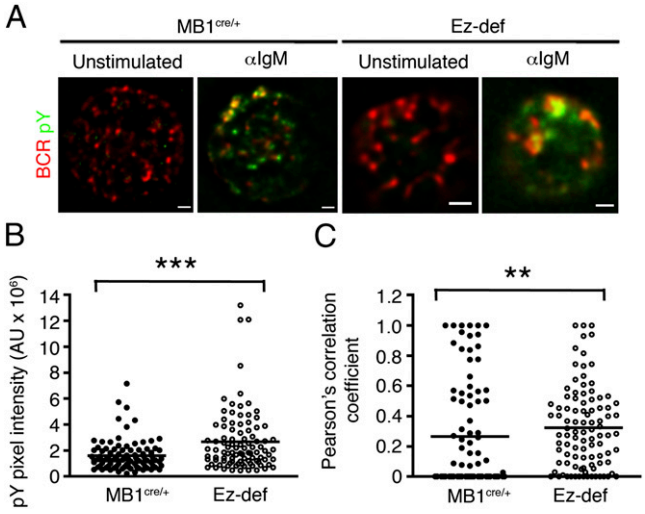

FIGURE 5. Larger BCR microclusters formed in the absence of ezrin are capable of signaling. (**A**) MB1$^{cre/+}$ and Ez-def B cells were left unstimulated or stimulated with 10 μg/ml anti-IgM for 3 min, stained for BCR (red) and tyrosine-phosphorylated proteins (pY; green), and imaged by epifluorescence microscopy. Merged images of BCR clusters at the surface and pY proteins are shown. Individual clusters formed after 3 min were quantified for pixel intensity of pY (mean ± SEM) (**B**) and Pearson correlation coefficient for BCR and pY (**C**). Scale bar, 1 μm. Data are representative of two independent experiments with ~15–35 cells imaged per experiment and 100–200 individual clusters per experiment analyzed for quantification. $^{**}p = 0.001$–0.01, $^{***}p < 0.001$.

Increase in B cell proliferation, differentiation, and Ab production in the absence of ezrin

Because Ez-def B cells exhibited stronger anti-IgM–induced BCR signaling ex vivo, we tested whether this translated to an enhanced ability to proliferate and differentiate into Ab-secreting cells (ASCs). We labeled purified MB1$^{cre/+}$ and Ez-def B cells with CFSE and stimulated them with anti-IgM for 5 d. Ez-def B cells showed higher CFSE dilution than did MB1$^{cre/+}$ B cells (Fig. 8A), and the number of dividing cells at each generation was greater for Ez-def B cells than for MB1$^{cre/+}$ B cells (Fig. 8B). To examine their differentiation into ASCs, we stimulated LPS-primed MB1$^{cre/+}$ and Ez-def B cells with anti-IgM ex vivo and quantified IgM- and IgG-secreting cells by ELISPOT. Anti-IgM–stimulated Ez-def B cells generated more spots than did MB1$^{cre/+}$ B cells (Fig. 8C), reflecting a 2-fold increase in differentiation into ASCs (Fig. 8D). To test whether the increase in the magnitude of ex vivo activation of Ez-def B cells was functionally relevant in vivo, we immunized MB1$^{cre/+}$ and Ez-def mice with NP-Ficoll, a T cell–independent Ag. Consistent with stronger BCR signaling, ERK activation, and B cell proliferation observed in purified Ez-def B cells, Ez-def mice produced more NP-specific IgM than did MB1$^{cre/+}$ mice early on (day 7); however, their responses were similar at later time points (days 14, 21, and 28) (Fig. 9A). To test whether increased BCR activation and MHC class II expression in Ez-def B cells affected their ability to mount T cell–dependent Ab responses, we immunized MB1$^{cre/+}$ and Ez-def mice with NP-CGG using LPS as an adjuvant. Although there was no difference in the production of NP-specific IgM by MB1$^{cre/+}$ and Ez-def mice at days 7 and 14, the response of MB1$^{cre/+}$ mice was diminished at days 21 and 28, whereas Ez-def mice showed sustained generation of NP-specific IgM (Fig. 9B). Ag-specific IgG1 and IgG2a (Fig. 9C, 9D) were higher in Ez-def mice, but IgG2b and IgG3 were not altered (Fig. 9E, 9F).

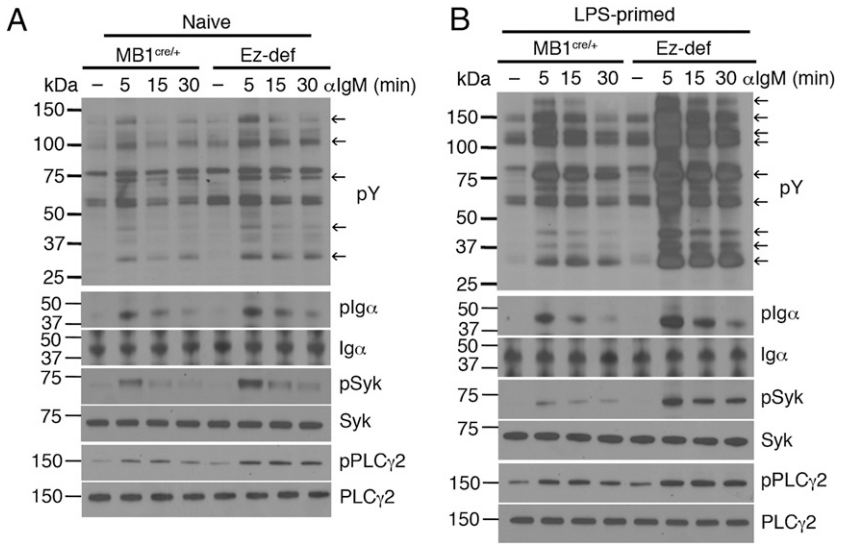

FIGURE 6. Loss of ezrin results in stronger proximal BCR signaling. Naive (**A**) or LPS-primed (**B**) MB1$^{cre/+}$ and Ez-def B cells were stimulated with 10 μg/ml of anti-IgM for the indicated times, and lysates were probed for phosphotyrosine (pY), and phosphorylated and total Igα, Syk, and PLCγ2. Representative blots from three independent experiments are shown. Arrows in the pY blot indicate bands with higher tyrosine phosphorylation.

Taken together, our data from high-resolution imaging, biochemical analysis of B cell activation, and in vivo immunization support a role for ezrin in modulating the magnitude of humoral immunity.

Discussion

In this study, we demonstrate that the plasma membrane–actin cytoskeleton cross-linking protein ezrin tunes the strength of B cell activation and Ab response. B cells lacking ezrin form larger and more stable BCR microclusters that recruit more tyrosine-phosphorylated proteins. In the absence of ezrin, B cells respond to Ag by undergoing stronger activation of proximal signaling mediators and the ERK pathway, as well as exhibit increased proliferation and differentiation into ASCs. In vivo, the absence of ezrin results in a magnified humoral response to immunization. Collectively, our data demonstrate a role for ezrin in limiting lipid raft dynamics and growth of BCR microclusters during the earliest phases of BCR-mediated B cell activation, revealing a novel mechanism for regulation of BCR signal amplification. Moreover, our study supports the notion that functional outcomes of Ag recognition by the BCR are encoded in its dynamics and modulated by membrane-cytoskeletal remodeling proteins.

Previous studies reporting live imaging of ezrin and BCR by TIRF microscopy delineated two spatiotemporal phases that limit BCR motility upon Ag binding (20). In the first phase, threonine dephosphorylation of ezrin and moesin leads to breakdown of barriers that normally limit BCR diffusion. Continued BCR stimulation and rephosphorylation of ERM proteins mark the second phase, in which the plasma membrane is relinked with cortical actin, and ERM-based corrals are reformed (20). As is evident from our STORM imaging data, the BCR diffusion coefficient was unchanged in the absence of ezrin when B cells were not stimulated. This suggests that ezrin is not required for limiting BCR diffusion in the steady-state and that its role in controlling this aspect of BCR dynamics may be redundant with that of the related protein moesin. In contrast, our data from both STORM and conventional TIRF imaging showed an increase in the size and intensity of BCR microclusters in the absence of ezrin, amounting to the presence of more BCRs per cluster. This is likely due to ineffective BCR confinement in the absence of ezrin, which may not be compensated for completely by moesin. These data suggest an important role for ezrin-based corrals in preventing an uncontrolled increase in BCR microcluster size and associated signaling. The bigger BCR microclusters in Ez-def B cells move with slower trajectories compared with those in MB1$^{cre/+}$ B cells, which may result from their overall "heaviness." One consequence of the slower mobility of "heavier" BCR clusters in Ez-def B cells was that they could be visualized at the cell surface for a greater number of frames than in MB1$^{cre/+}$ cells. This indicated that the

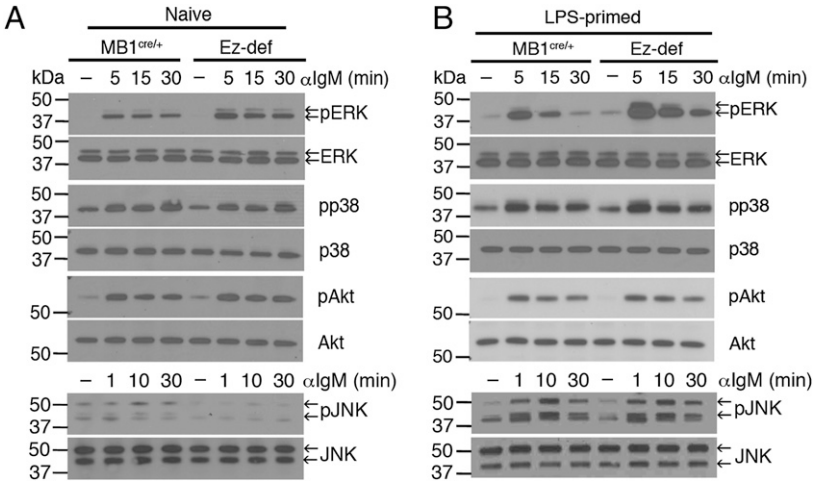

FIGURE 7. Ez-def B cells show increased ERK activation. Naive (**A**) or LPS-primed (**B**) MB1$^{cre/+}$ and Ez-def B cells were stimulated with anti-IgM for the indicated times, and lysates were probed for phosphorylated and total ERK, p38, Akt, and JNK. Representative blots from three independent experiments are shown. Arrows indicate the p44/p42 isoforms of ERK and p54/p46 isoforms of JNK.

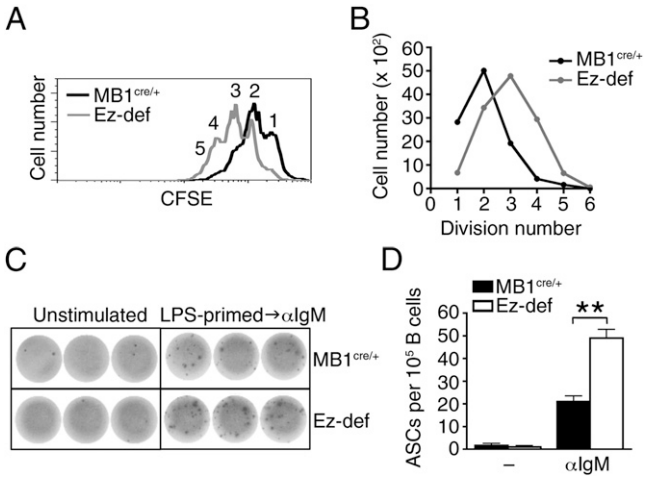

FIGURE 8. Absence of ezrin leads to increased B cell proliferation and differentiation into ASCs. (**A**) CFSE-labeled MB1$^{cre/+}$ and Ez-def B cells were cultured with anti-IgM for 5 d followed by flow cytometry. A representative of three independent experiments is shown. (**B**) Number of cells at each cell division [numbered 1–5 in (A)]. LPS-primed MB1$^{cre/+}$ and Ez-def B cells were stimulated with anti-IgM for 24 h, and ASCs were quantified by ELISPOT assay. (**C**) Spots of IgM or IgG Ab-secreting B cells. (**D**) Number of ASCs/10^5 B cells. The data are representative of two independent experiments (mean ± SEM is shown). $^{**}p = 0.001–0.01$.

BCR microclusters were more stable in the absence of ezrin, which is also the likely reason for delayed BCR capping in Ez-def B cells. An overall increase in BCR signaling, proliferation, and differentiation observed in Ez-def anti-IgM–stimulated B cells further supports a role for ezrin in limiting the overall strength of BCR signaling by limiting the growth and stability of BCR clusters.

Single-particle–tracking studies demonstrated that Ag-bound BCRs oligomerize and immobilize and this is when they transduce biochemical signals through recruitment of key signaling mediators (29). Entry of oligomerized BCRs into cholesterol and glycosphingolipid-rich lipid raft domains (30–32) was suggested as one of the mechanisms of initiation of BCR signaling because BCR and lipid raft colocalization bring the raft-localized Src family kinases in close proximity to their substrates (3, 33). At the same time, BCR stimulation induces rapid dephosphorylation of ezrin at T567, delinking the lipid rafts and plasma membrane from cortical actin filaments and inducing lipid raft coalescence (18). Lower velocity and diffusion constant of BCR clusters observed in the absence of ezrin suggested that they would support stronger signaling. This was confirmed by our finding that the bigger BCR clusters formed in Ez-def B cells are associated with more tyrosine-phosphorylated proteins. Our data showed that lipid raft coalescence was also enhanced in B cells lacking ezrin expression, suggesting a model wherein increased raft coalescence and stability of larger BCR clusters could jointly provide a bigger platform for initiation of tyrosine phosphorylation. Our observation that global tyrosine phosphorylation, including that of Igα, Syk, and PLCγ, is increased in the absence of ezrin is consistent with this model. Interestingly, despite an overall increase in tyrosine phosphorylation of proximal signaling proteins, distal signaling pathways showed variable sensitivity to the absence of ezrin. Activation of p38 and PI3K was unaffected in Ez-def B cells, revealing differential requirement and sensitivity of these arms of BCR signaling to regulation by ezrin. In contrast, lower JNK activation in naive Ez-def B cells supports the requirement for

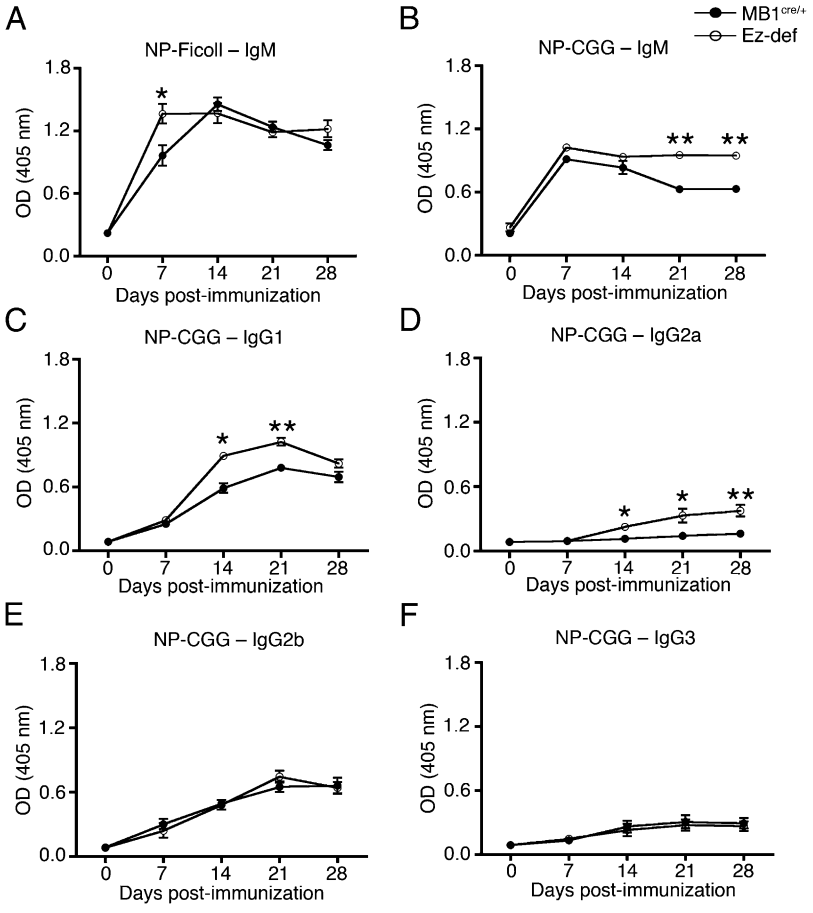

FIGURE 9. Ez-def mice produce higher levels of Ag-specific Igs. MB1$^{cre/+}$ and Ez-def mice were immunized with NP-Ficoll (**A**) or NP-CGG with LPS as adjuvant (**B**–**F**), and serum levels of NP-specific IgM (A, B), IgG1 (C), IgG2a (D), IgG2b (E), and IgG3 (F) Abs were quantified. Data are representative of two independent experiments (mean ± SEM). $^{*}p = 0.01–0.05$, $^{**}p = 0.001–0.01$.

tyrosine-phosphorylated ezrin in spatially connecting the BCR signalosome to endosomal JNK activation (22). ERK activation was robustly increased in the absence of ezrin, indicating a linear relationship between proximal signaling proteins and ERK activation. Ezrin was also shown to regulate ERK activation in T cells, albeit through a different mechanism. In T cells, ezrin interacts with the PDZ domain–containing scaffold protein Dlg1 (34), which localizes to the immunological synapse and associates with several TCR signaling proteins (35). Upon knockdown of ezrin expression, the TCR stimulation–induced radial distribution of microtubules was lost, and the TCR microclusters became larger as a result of compromised centripetal movement (34). Our data support a role for ezrin in restricting ERK activation through a membrane-proximal effect on BCR microclustering mediated by ezrin-rich barriers. Although ezrin appears to use distinct mechanisms to limit the overall T and B lymphocyte response to Ag, it remains to be tested whether microtubule dynamics are altered in Ez-def B cells and whether they additionally contribute to an increase in BCR cluster size and ERK phosphorylation through a Dlg-dependent mechanism. Ez-def mice exhibited an increase in Ab production compared with MB1$^{cre/+}$ mice, which is consistent with the overall increase in the activation of B cells in the absence of ezrin. ERK signaling regulates B cell proliferation (36) and Blimp-1 expression and is critical for the generation of plasma cells from germinal center B cells (37), supporting the correlation among increased anti-IgM–induced ERK activation, proliferation, differentiation into ASCs, and higher Ag-specific Ab production in Ez-def mice.

We observed that T cell–dependent Ab production was also higher in the absence of ezrin. Because dephosphorylation of ERM proteins in T cells reduces cellular rigidity, leading to more efficient T cell–APC conjugate formation (38), it is possible that the absence of ezrin in B cells leads to similar changes in membrane flexibility, making them better Ag presenters to T cells. Thus, T–B interactions in the germinal centers may also be subject to ezrin-mediated regulation. Our data showing an increase in lipid raft coalescence in Ez-def B cells support this view. We observed that MHC class II expression is higher in resting Ez-def B cells; this feature may further contribute to their improved engagement with T cells (39) and result in increased T cell help. None of the other cell surface proteins, such as CD19, CD21, CD40, and CD62L, showed alterations in their steady-state expression level in the absence of ezrin, indicating a specific mechanism that enables ezrin to regulate surface MHC class II levels. MHC class II expression is subject to several types of regulation, including transcription, intracellular transport, and ubiquitin-mediated degradation (40–43). The guanine nucleotide exchange factor Vav, which is known to activate actin cytoskeletal rearrangements, was also shown to regulate MHC class II transport in both resting and activated B cells (40). Vav also has a positive role in transcriptional activation of MHC class II regulatory factors, such as CIITA (40). The absence of ezrin may increase Vav activity, thereby mobilizing more MHC class II molecules from intracellular compartments to the cell surface. Alternately, increased activation of Vav in Ez-def B cells may lead to higher transcription of MHC class II genes. Another mechanism of MHC class II cell surface expression described recently relates to its degradation by membrane-associated ring–CH 1 (MARCH1) protein, which has an E3 ubiquitin ligase activity (41, 42). MHC class II complex is a target of MARCH1-mediated ubiquitination and degradation in B cells (41), and MARCH1-deficient B cells show upregulation of MHC class II expression (41). Because MARCH1 is a membrane-associated protein, it is attractive to speculate that the presence of ezrin in the cell cortex may stabilize it either through direct binding or through another adaptor protein. It will be interesting to test whether loss of ezrin reduces MARCH1 levels in the B cell membrane and, thus, prevents MARCH1-mediated degradation of MHC class II.

Regardless of the mechanism, higher MHC class II expression may serve to recruit more T cell help. It is well established that T cell help to B cells aids in their affinity maturation, generation of memory, and class-switch recombination (44, 45). This raises an important question: whether stronger Ag-specific IgG production in Ez-def B cells is only due to global increase in B cell activation or whether higher class switching also plays a role. The time during an ongoing immune response at which Ag-specific IgM and IgG Abs can be detected serves as an approximate determinant of class switching. We observed that NP-specific IgM, IgG1, and IgG2a levels were higher in Ez-def mice compared with MB1$^{cre/+}$ mice immunized with NP-CGG. However, the difference in NP-specific IgM levels was only statistically significant at days 21 and 28 of immunization. At day 14, the NP-specific IgM levels were comparable in both groups of mice, but NP-specific IgG1 and IgG2a were higher in Ez-def mice, indicating increased B cell class switching in the absence of ezrin at this early phase of the immune response. Quantitative detection of switch circles in B cells will greatly aid in addressing the role of ezrin in class switching. It also will be interesting to test whether the repertoire of BCR affinities generated upon immunization of Ez-def mice is different from that of MB1$^{cre/+}$ mice, as well as whether memory responses are altered upon loss of ezrin in B cells.

The conditional genetic deletion of ezrin did not affect bone marrow B cell development, which is consistent with the lack of developmental defects in lymphocytes of moesin-deficient mice (46) and with unaltered thymic T cell development in mice with conditional deletion of ezrin in CD4$^+$ T cells (47). Systemic deficiency of ezrin was shown to result in lower B and T cell numbers, but this difference was attributed to systemic malnutrition, which also accounted for neonatal lethality of mice (48). Given the collaboration between ezrin and moesin in regulating BCR diffusion dynamics (20), we expect that additional loss of moesin in Ez-def mice will further enhance BCR activation and functional responses. This prediction is supported by the demonstration that the defect in IL-2 secretion observed in mature T cells that lack ezrin is exacerbated by additional loss of moesin (47).

We reported previously that chemokines induce transient dephosphorylation of ezrin at T567, which is important for B cell migration (21). This involves resorption of microvilli as ezrin undergoes dephosphorylation and reorientation of ezrin to the lamellipodial region for rapid evolution of cell–substratum contacts at the front of migrating B cells (21). In the current study, the absence of ezrin did not affect the homeostasis of major B cell subsets in the steady-state, but it remains to be tested whether homing of Ez-def and MB1$^{cre/+}$ B cells would be comparable or different in a competitive assay involving cotransfer of cells into mice. Our expectation is that absence of ezrin will lead to reduced in vivo homing. This is based on the demonstration that mice lacking ERM proteins in mature T cells display decreased homing to lymphoid organs (49) and that transgenic mice expressing a constitutively active mutant of ezrin in T cells have defects in transendothelial T cell migration due to an increase in membrane tension (50). We have demonstrated that treatment of naive B cells with different stimuli, such as Ag, chemokines, LPS, and CD40L, results in dephosphorylation of T567 in ezrin, whereas phosphorylation at Y353 is only induced upon BCR cross-linking (22). This indicates a common unifying role for ezrin-dependent membrane-cytoskeletal remodeling in the response of B cells in a variety of contexts. Therefore, loss of ezrin in B cells has the potential to impact multiple B cell processes, such as cell migration, acquisition

of T cell help, and innate responses to pathogens. Our preliminary findings indicate that this is indeed the case. The strength of BCR signaling and outcome of Ag challenge are also known to be regulated by coreceptors that operate in proximity of the BCR. For example, CD19 and CD21 function together to sustain BCR signaling in the lipid raft environment (51). Localization of the tripartite complex consisting of the BCR and its coreceptors CD19 and CD21 in lipid rafts is promoted by the tetraspanin protein CD81 (52). The molecular basis of colocalization of BCR with CD19 and the role of CD81 in this phenomenon was described recently by Mattila et al. (53), who used superresolution microscopy to demonstrate that CD81 collaborates with the actin cytoskeleton to organize BCR clusters and regulate BCR signaling. A direct role for ezrin in modulating CD81 function is predicted by the observation that cross-linking of CD81 induces Syk-dependent Y353 phosphorylation of ezrin, leading to their colocalization with F-actin (54). Given the joint regulation of BCR clusters by ezrin and actin networks (20), it is conceivable that the multimolecular assembly of BCR and its coreceptors will be altered in the absence of ezrin and result in further fine tuning of B cell responses. As ezrin tunes BCR signaling and humoral immunity, Ez-def mice also represent a novel tool to examine the significance of membrane-cytoskeletal remodeling in B cell tolerance, autoimmunity, and malignancy.

Acknowledgments

We thank the Lerner Research Institute Imaging Core personnel for assistance with image analysis.

Disclosures

The authors have no financial conflicts of interest.

References

1. Pillai, S., and A. Cariappa. 2009. The follicular versus marginal zone B lymphocyte cell fate decision. *Nat. Rev. Immunol.* 9: 767–777.
2. Kurosaki, T., H. Shinohara, and Y. Baba. 2010. B cell signaling and fate decision. *Annu. Rev. Immunol.* 28: 21–55.
3. Gupta, N., and A. L. DeFranco. 2007. Lipid rafts and B cell signaling. *Semin. Cell Dev. Biol.* 18: 616–626.
4. Lund, F. E., and T. D. Randall. 2010. Effector and regulatory B cells: modulators of CD4+ T cell immunity. *Nat. Rev. Immunol.* 10: 236–247.
5. Lampropoulou, V., E. Calderon-Gomez, T. Roch, P. Neves, P. Shen, U. Stervbo, P. Boudinot, S. M. Anderton, and S. Fillatreau. 2010. Suppressive functions of activated B cells in autoimmune diseases reveal the dual roles of Toll-like receptors in immunity. *Immunol. Rev.* 233: 146–161.
6. DiLillo, D. J., T. Matsushita, and T. F. Tedder. 2010. B10 cells and regulatory B cells balance immune responses during inflammation, autoimmunity, and cancer. *Ann. N. Y. Acad. Sci.* 1183: 38–57.
7. Burdin, N., F. Rousset, and J. Banchereau. 1997. B-cell-derived IL-10: production and function. *Methods* 11: 98–111.
8. Liossis, S. N., B. Kovacs, G. Dennis, G. M. Kammer, and G. C. Tsokos. 1996. B cells from patients with systemic lupus erythematosus display abnormal antigen receptor-mediated early signal transduction events. *J. Clin. Invest.* 98: 2549–2557.
9. Davis, R. E., V. N. Ngo, G. Lenz, P. Tolar, R. M. Young, P. B. Romesser, H. Kohlhammer, L. Lamy, H. Zhao, Y. Yang, et al. 2010. Chronic active B-cell-receptor signalling in diffuse large B-cell lymphoma. *Nature* 463: 88–92.
10. Woyach, J. A., A. J. Johnson, and J. C. Byrd. 2012. The B-cell receptor signaling pathway as a therapeutic target in CLL. *Blood* 120: 1175–1184.
11. Tolar, P., H. W. Sohn, W. Liu, and S. K. Pierce. 2009. The molecular assembly and organization of signaling active B-cell receptor oligomers. *Immunol. Rev.* 232: 34–41.
12. Liu, W., T. Meckel, P. Tolar, H. W. Sohn, and S. K. Pierce. 2010. Intrinsic properties of immunoglobulin IgG1 isotype-switched B cell receptors promote microclustering and the initiation of signaling. *Immunity* 32: 778–789.
13. Davey, A. M., and S. K. Pierce. 2012. Intrinsic differences in the initiation of B cell receptor signaling favor responses of human IgG(+) memory B cells over IgM(+) naive B cells. *J. Immunol.* 188: 3332–3341.
14. Liu, W., T. Meckel, P. Tolar, H. W. Sohn, and S. K. Pierce. 2010. Antigen affinity discrimination is an intrinsic function of the B cell receptor. *J. Exp. Med.* 207: 1095–1111.
15. Tsourkas, P. K., W. Liu, S. C. Das, S. K. Pierce, and S. Raychaudhuri. 2012. Discrimination of membrane antigen affinity by B cells requires dominance of kinetic proofreading over serial engagement. *Cell. Mol. Immunol.* 9: 62–74.
16. Pierce, S. K., and W. Liu. 2010. The tipping points in the initiation of B cell signalling: how small changes make big differences. *Nat. Rev. Immunol.* 10: 767–777.
17. Fehon, R. G., A. I. McClatchey, and A. Bretscher. 2010. Organizing the cell cortex: the role of ERM proteins. *Nat. Rev. Mol. Cell Biol.* 11: 276–287.
18. Gupta, N., B. Wollscheid, J. D. Watts, B. Scheer, R. Aebersold, and A. L. DeFranco. 2006. Quantitative proteomic analysis of B cell lipid rafts reveals that ezrin regulates antigen receptor-mediated lipid raft dynamics. *Nat. Immunol.* 7: 625–633.
19. Treanor, B., D. Depoil, A. Gonzalez-Granja, P. Barral, M. Weber, O. Dushek, A. Bruckbauer, and F. D. Batista. 2010. The membrane skeleton controls diffusion dynamics and signaling through the B cell receptor. *Immunity* 32: 187–199.
20. Treanor, B., D. Depoil, A. Bruckbauer, and F. D. Batista. 2011. Dynamic cortical actin remodeling by ERM proteins controls BCR microcluster organization and integrity. *J. Exp. Med.* 208: 1055–1068.
21. Parameswaran, N., K. Matsui, and N. Gupta. 2011. Conformational switching in ezrin regulates morphological and cytoskeletal changes required for B cell chemotaxis. *J. Immunol.* 186: 4088–4097.
22. Parameswaran, N., G. Enyindah-Asonye, N. Bagheri, N. B. Shah, and N. Gupta. 2013. Spatial coupling of JNK activation to the B cell antigen receptor by tyrosine-phosphorylated ezrin. *J. Immunol.* 190: 2017–2026.
23. Curto, M., and A. I. McClatchey. 2004. Ezrin...a metastatic detERMinant? *Cancer Cell* 5: 113–114.
24. Saotome, I., M. Curto, and A. I. McClatchey. 2004. Ezrin is essential for epithelial organization and villus morphogenesis in the developing intestine. *Dev. Cell* 6: 855–864.
25. Hobeika, E., S. Thiemann, B. Storch, H. Jumaa, P. J. Nielsen, R. Pelanda, and M. Reth. 2006. Testing gene function early in the B cell lineage in mb1-cre mice. *Proc. Natl. Acad. Sci. USA* 103: 13789–13794.
26. Matsui, K., N. Parameswaran, N. Bagheri, B. Willard, and N. Gupta. 2011. Proteomics analysis of the ezrin interactome in B cells reveals a novel association with Myo18aα. *J. Proteome Res.* 10: 3983–3992.
27. Rust, M. J., M. Bates, and X. Zhuang. 2006. Sub-diffraction-limit imaging by stochastic optical reconstruction microscopy (STORM). *Nat. Methods* 3: 793–795.
28. Veatch, S. L., B. B. Machta, S. A. Shelby, E. N. Chiang, D. A. Holowka, and B. A. Baird. 2012. Correlation functions quantify super-resolution images and estimate apparent clustering due to over-counting. *PLoS ONE* 7: e31457.
29. Tolar, P., J. Hanna, P. D. Krueger, and S. K. Pierce. 2009. The constant region of the membrane immunoglobulin mediates B cell-receptor clustering and signaling in response to membrane antigens. *Immunity* 30: 44–55.
30. Cheng, P. C., B. K. Brown, W. Song, and S. K. Pierce. 2001. Translocation of the B cell antigen receptor into lipid rafts reveals a novel step in signaling. *J. Immunol.* 166: 3693–3701.
31. Cheng, P. C., M. L. Dykstra, R. N. Mitchell, and S. K. Pierce. 1999. A role for lipid rafts in B cell antigen receptor signaling and antigen targeting. *J. Exp. Med.* 190: 1549–1560.
32. Gupta, N., and A. L. DeFranco. 2003. Visualizing lipid raft dynamics and early signaling events during antigen receptor-mediated B-lymphocyte activation. *Mol. Biol. Cell* 14: 432–444.
33. Dykstra, M. L., A. Cherukuri, and S. K. Pierce. 2001. Floating the raft hypothesis for immune receptors: access to rafts controls receptor signaling and trafficking. *Traffic* 2: 160–166.
34. Lasserre, R., S. Charrin, C. Cuche, A. Danckaert, M. I. Thoulouze, F. de Chaumont, T. Duong, N. Perrault, N. Varin-Blank, J. C. Olivo-Marin, et al. 2010. Ezrin tunes T-cell activation by controlling Dlg1 and microtubule positioning at the immunological synapse. *EMBO J.* 29: 2301–2314.
35. Xavier, R., S. Rabizadeh, K. Ishiguro, N. Andre, J. B. Ortiz, H. Wachtel, D. G. Morris, M. Lopez-Ilasaca, A. C. Shaw, W. Swat, and B. Seed. 2004. Discs large (Dlg1) complexes in lymphocyte activation. *J. Cell Biol.* 166: 173–178.
36. Dong, C., R. J. Davis, and R. A. Flavell. 2002. MAP kinases in the immune response. *Annu. Rev. Immunol.* 20: 55–72.
37. Yasuda, T., K. Kometani, N. Takahashi, Y. Imai, Y. Aiba, and T. Kurosaki. 2011. ERKs induce expression of the transcriptional repressor Blimp-1 and subsequent plasma cell differentiation. *Sci. Signal.* 4: ra25.
38. Faure, S., L. I. Salazar-Fontana, M. Semichon, V. L. Tybulewicz, G. Bismuth, A. Trautmann, R. N. Germain, and J. Delon. 2004. ERM proteins regulate cytoskeleton relaxation promoting T cell-APC conjugation. *Nat. Immunol.* 5: 272–279.
39. Blum, J. S., P. A. Wearsch, and P. Cresswell. 2013. Pathways of antigen processing. *Annu. Rev. Immunol.* 31: 443–473.
40. Jux, B., A. Staratschek-Jox, J. M. Penninger, J. L. Schultze, and W. Kolanus. 2013. Vav1 regulates MHCII expression in murine resting and activated B cells. *Int. Immunol.* 25: 307–317.
41. Galbas, T., V. Steimle, R. Lapointe, S. Ishido, and J. Thibodeau. 2012. MARCH1 down-regulation in IL-10-activated B cells increases MHC class II expression. *Cytokine* 59: 27–30.
42. Thibodeau, J., M. C. Bourgeois-Daigneault, G. Huppé, J. Tremblay, A. Aumont, M. Houde, E. Bartee, A. Brunet, M. E. Gauvreau, A. de Gassart, et al. 2008. Interleukin-10-induced MARCH1 mediates intracellular sequestration of MHC class II in monocytes. *Eur. J. Immunol.* 38: 1225–1230.
43. Reith, W., and B. Mach. 2001. The bare lymphocyte syndrome and the regulation of MHC expression. *Annu. Rev. Immunol.* 19: 331–373.
44. Crotty, S. 2012. The 1-1-1 fallacy. *Immunol. Rev.* 247: 133–142.

45. Xu, Z., H. Zan, E. J. Pone, T. Mai, and P. Casali. 2012. Immunoglobulin class-switch DNA recombination: induction, targeting and beyond. *Nat. Rev. Immunol.* 12: 517–531.
46. Hirata, T., A. Nomachi, K. Tohya, M. Miyasaka, S. Tsukita, T. Watanabe, and S. Narumiya. 2012. Moesin-deficient mice reveal a non-redundant role for moesin in lymphocyte homeostasis. *Int. Immunol.* 24: 705–717.
47. Shaffer, M. H., R. S. Dupree, P. Zhu, I. Saotome, R. F. Schmidt, A. I. McClatchey, B. D. Freedman, and J. K. Burkhardt. 2009. Ezrin and moesin function together to promote T cell activation. *J. Immunol.* 182: 1021–1032.
48. Shaffer, M. H., Y. Huang, E. Corbo, G. F. Wu, M. Velez, J. K. Choi, I. Saotome, J. L. Cannon, A. I. McClatchey, A. I. Sperling, et al. 2010. Ezrin is highly expressed in early thymocytes, but dispensable for T cell development in mice. *PLoS ONE* 5: e12404.
49. Chen, E. J., M. H. Shaffer, E. K. Williamson, Y. Huang, and J. K. Burkhardt. 2013. Ezrin and moesin are required for efficient T cell adhesion and homing to lymphoid organs. *PLoS ONE* 8: e52368.
50. Liu, Y., N. V. Belkina, C. Park, R. Nambiar, S. M. Loughhead, G. Patino-Lopez, K. Ben-Aissa, J. J. Hao, M. J. Kruhlak, H. Qi, et al. 2012. Constitutively active ezrin increases membrane tension, slows migration, and impedes endothelial transmigration of lymphocytes in vivo in mice. *Blood* 119: 445–453.
51. Cherukuri, A., P. C. Cheng, H. W. Sohn, and S. K. Pierce. 2001. The CD19/CD21 complex functions to prolong B cell antigen receptor signaling from lipid rafts. *Immunity* 14: 169–179.
52. Cherukuri, A., T. Shoham, H. W. Sohn, S. Levy, S. Brooks, R. Carter, and S. K. Pierce. 2004. The tetraspanin CD81 is necessary for partitioning of coligated CD19/CD21-B cell antigen receptor complexes into signaling-active lipid rafts. *J. Immunol.* 172: 370–380.
53. Mattila, P. K., C. Feest, D. Depoil, B. Treanor, B. Montaner, K. L. Otipoby, R. Carter, L. B. Justement, A. Bruckbauer, and F. D. Batista. 2013. The actin and tetraspanin networks organize receptor nanoclusters to regulate B cell receptor-mediated signaling. *Immunity* 38: 461–474.
54. Coffey, G. P., R. Rajapaksa, R. Liu, O. Sharpe, C. C. Kuo, S. W. Krauss, Y. Sagi, R. E. Davis, L. M. Staudt, J. P. Sharman, et al. 2009. Engagement of CD81 induces ezrin tyrosine phosphorylation and its cellular redistribution with filamentous actin. *J. Cell Sci.* 122: 3137–3144.